



**HAL**  
open science

## Helically forced MHD flows in confined cylindrical geometries

Malcolm Roberts, Matthieu Leroy, Jorge Morales, Wouter J.T. Bos, Kai Schneider

► **To cite this version:**

Malcolm Roberts, Matthieu Leroy, Jorge Morales, Wouter J.T. Bos, Kai Schneider. Helically forced MHD flows in confined cylindrical geometries. *Fluid Dynamics Research*, 2014, 46, pp.061422. 10.1088/0169-5983/46/6/061422 . hal-01005421

**HAL Id: hal-01005421**

**<https://hal.science/hal-01005421>**

Submitted on 12 Jun 2014

**HAL** is a multi-disciplinary open access archive for the deposit and dissemination of scientific research documents, whether they are published or not. The documents may come from teaching and research institutions in France or abroad, or from public or private research centers.

L'archive ouverte pluridisciplinaire **HAL**, est destinée au dépôt et à la diffusion de documents scientifiques de niveau recherche, publiés ou non, émanant des établissements d'enseignement et de recherche français ou étrangers, des laboratoires publics ou privés.

# Helically forced MHD flows in confined cylindrical geometries

Malcolm Roberts<sup>1</sup>, Matthieu Leroy<sup>1</sup>, Jorge Morales<sup>2</sup>,  
Wouter Bos<sup>2</sup>, Kai Schneider<sup>1</sup>‡

<sup>1</sup>M2P2, Aix-Marseille University, 38 Rue Frédéric Joliot-Curie 13451 Marseille, Cedex 20, France

<sup>2</sup>LMFA, Ecole Centrale de Lyon, UMR 5509, CNRS, Université de Lyon, 69134 Ecully, France

**Abstract.** The dynamics of a magnetically forced conducting fluid in confined geometries is studied. A pseudospectral method with volume penalisation is used to solve the resistive magnetohydrodynamic (MHD) equations. A helical magnetic field is imposed via boundary conditions, which generates a response in the velocity field for large enough magnitudes. Different helical structures are observed in the flow depending on the magnitude and direction of the forcing and the cross-sectional geometry of the fluid domain. A computational technique for finding a solenoidal vector field which can be used in complex geometries is also proposed.

*Keywords:* MHD, self-organization, confined geometry, volume penalisation

‡ Corresponding author, [kschneid@cmi.univ-mrs.fr](mailto:kschneid@cmi.univ-mrs.fr)

## 1. Introduction

Vortical structure formation plays an important role in magnetohydrodynamic (MHD) flows in a variety of settings and applications, such as the Earth's core (Moffatt 1978), metal casting, and fusion devices of the Reversed Field Pinch type (Taylor 1974) and of the tokamak type (Wesson 2011). The development of large rotational structures has been addressed before in (Neffaa, Bos & Schneider 2008, Bos, Neffaa & Schneider 2008). While some analytic results exist for MHD flows, we must generally rely on numerical simulations in order to understand the behaviour of those fluids in confined geometries. Understanding structures in MHD flows lends insight into the underlying mathematical properties and can help to control MHD flows more efficiently.

In this paper we explore the behaviour of a conducting fluid and the evolution of the flow topology under the influence of external magnetic forcing in two cylindrical geometries. In previous investigations we focused on the structure formation of magnetofluids in two-dimensional (Neffaa et al. 2008, Bos et al. 2008) and toroidally confined (Morales, Bos, Schneider & Montgomery 2012) domains. The case of a cylindrical domain was considered numerically in (Shan, Montgomery & Chen 1991, Shan & Montgomery 1993*b*) in the case of non-penetration boundary conditions. This choice was necessary for these simulations because the fields were decomposed into eigenfunctions of the curl operator in order to observe the dynamics of helical structures, and it was argued, via an energy-minimisation argument, that the dominant mode of the flow is such a helical basis function. The instability threshold determined analytically was confirmed numerically and the evolution of the flow with the magnitude of the forcing was described. Due to the absence of an efficient physical-space to Chandrasekhar-Kendall function-space transform, the nonlinear term was computed directly, rapidly increasing the computational cost. In this paper, we use a pseudospectral method (Canuto, Hussaini, Quarteroni & Zang 1988) combined with a volume penalisation method for imposing boundary conditions in complex geometries (Arquis & Caltagirone 1984, Angot, Bruneau & Fabrie 1999). Thus we are able to implement different boundary conditions than used in (Shan et al. 1991) and to perform simulations in cylindrical geometries with different cross-sections. A related study, which was limited to circular cross-sections and for different parameters focusing on the Reversed Field Pinch application can be found in (Veranda, Bonfiglio, Cappello, Chacón & Escande 2013, Bonfiglio, Veranda, Cappello, Escande & Chacón 2013). The self-organization of compressible MHD flows into helical structures has also

been observed in (Zhu, Horiuchi, Sato et al. 1995) and (Horiuchi & Sato 1986), for example, where the mechanism of self-organization is magnetic re-connection.

This paper is organised as follows: in section 2 we give a mathematical description of the problem and present our numerical technique. In section 3, we explore the structure of the velocity field in a circular geometry when forced by an external helical magnetic field, and we show the effect of wrapping number in section 4. Section 6 shows how the flow topology changes when the cross-section is modified. We give our conclusions and future perspectives in section 7.

## 2. Mathematical Description and Numerical Method

### 2.1. Mathematical Description

Let  $\mathbf{u}$  denote the velocity and  $\mathbf{B}$  the magnetic field of the conducting fluid. The time evolution of these quantities using conventional, Alfvén normalised variables, is given by

$$\frac{\partial \mathbf{u}}{\partial t} = \mathbf{u} \times \boldsymbol{\omega} + \mathbf{j} \times \mathbf{B} - \nabla P + \nu \nabla^2 \mathbf{u} \quad (1)$$

$$\frac{\partial \mathbf{B}}{\partial t} = \nabla \times (\mathbf{u} \times \mathbf{B}) + \lambda \nabla^2 \mathbf{B} \quad (2)$$

where  $P$  is the total pressure,  $\boldsymbol{\omega} = \nabla \times \mathbf{u}$  is the vorticity, and  $\mathbf{j} = \nabla \times \mathbf{B}$  is the current density. Physical parameters are the kinematic viscosity  $\nu = 4.5 \times 10^{-2}$ , and the magnetic diffusivity  $\lambda = 4.5 \times 10^{-2}$ . Both the velocity and magnetic field are considered to be incompressible, so  $\nabla \cdot \mathbf{u} = 0$  and  $\nabla \cdot \mathbf{B} = 0$ .

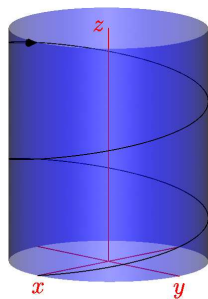


Figure 1: Sketch of the flow configuration: a conducting fluid in a cylinder is forced with a helical magnetic field imposed at the boundary.

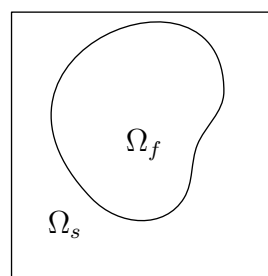


Figure 2: Schematic of fluid domain  $\Omega_f$  and penalised domain  $\Omega_s$  in computational domain  $\Omega = \Omega_f \cup \Omega_s$ .

The fluid is confined in a cylinder of length  $z_\ell = 8$  with its axis oriented along the  $z$ -axis. The ends of the cylinder are treated as periodic. The cross-section of the cylinder in the  $x$ - $y$  plane is either a circle of radius 1 or an ellipse with major radius 1 along the  $x$ -axis and minor radius  $1/\sqrt{2}$  along the  $y$  axis corresponding to an eccentricity of  $1/\sqrt{2}$ . No-slip (and non-penetration) boundary conditions are imposed on the velocity field. A helical forcing is imposed in the boundary conditions for  $\mathbf{B}$ , where the normal component is set to zero, the  $z$ -component is set to  $B_0$ , and the poloidal component is set to  $B_c$ . This corresponds to the boundary conditions for the magnetic field following a helix along the wall, as illustrated in Figure 1. We define the wrapping number  $q$  to be the number of rotations achieved by a magnetic streamline following the boundary conditions between  $z = 0$  and  $z = z_\ell$ , and we choose  $(B_0, B_c)$  pairs which provide integral values of  $q$  for the simulations in this paper. It was shown in (Shan & Montgomery 1993*b*, Shan & Montgomery 1993*a*) that the instability of the current setup is determined by two parameters: the Hartmann number and the pinch-ratio. The Hartmann number was chosen proportional to the axial magnetic field, and the pinch-ratio is proportional to the wrapping number. Our description in terms of  $B_0$  and  $q$  is thus equivalent to the previous investigations.

The magnetic field is initialised to a linear profile that matches the boundary conditions. The velocity field is set to an uncorrelated Gaussian solenoidal field using with kinetic energy of the order  $10^{-7}$ .

## 2.2. Numerical method

The numerical method used for the simulations we studied is a Fourier pseudospectral method, with boundary conditions implemented via the penalisation method. A detailed description of the code and its validation can be found in (Morales, Leroy, Bos & Schneider 2012, revised).

The cylinder is immersed in a computational domain consisting of a periodic box of dimensions  $x_\ell \times y_\ell \times z_\ell = 0.8\pi \times 0.8\pi \times 8$ , which we denote  $\Omega$ . The fluid domain is denoted  $\Omega_f$ , with the wall domain (also called solid domain) denoted  $\Omega_s$ , where  $\Omega = \Omega_f \cup \Omega_s$ , and  $|\Omega_f \cap \Omega_s| = 0$ . Let  $\chi$  be the characteristic function for  $\Omega_s$ . For the velocity, on which we impose homogeneous Dirichlet boundary conditions, we add  $-\frac{1}{\eta}\chi\mathbf{u}$  to the right-hand side of equation (1), where  $\eta$  is the penalisation parameter. We determine  $P$  by first computing the nonlinear source term  $\mathbf{S}\mathbf{u} = \mathbf{u} \times \boldsymbol{\omega} + \mathbf{j} \times \mathbf{B} - \frac{1}{\eta}\chi\mathbf{u}$  and solving the Poisson equation  $\nabla^2 P = \nabla \cdot \mathbf{S}\mathbf{u}$ . Substituting the resulting pressure gradient into equation (1) enforces  $\nabla \cdot \mathbf{u} = 0$ .

For the magnetic field, we first find the penalisation field  $\mathbf{B}_s$  which matches the helical-forcing boundary conditions on  $\partial\Omega_f$  and which is solenoidal in  $\Omega$ . A method for generating this field is given in Appendix A. We impose boundary conditions on  $\mathbf{B}$  by adding  $-\frac{1}{\eta}\chi(\mathbf{B} - \mathbf{B}_s)$  to equation (2). In order to ensure that  $\nabla \cdot \mathbf{B} = 0$ , we time-step by first computing  $\mathbf{S}_B = \nabla \times (\mathbf{u} \times \mathbf{B}) - \frac{1}{\eta}\chi(\mathbf{B} - \mathbf{B}_s)$  and projecting  $\mathbf{S}_B$  onto the solenoidal manifold via a Helmholtz projection, which removes any divergence introduced by the penalisation term. Note that the penalisation field is itself solenoidal; this implies that the only source of divergence is due to presence of  $\chi$  in the penalisation term. A detailed validation of the penalisation method to impose tangential forcing at the boundary can be found in (Morales et al. 2012, revised) for Taylor-Couette flow. In contrast to (Morales et al. 2012), we penalise the magnetic field in the entire computational domain in order to avoid discontinuities in the nonlinear source term.

The resulting equations are advanced in time in Fourier space using a second-order Adams-Bashforth method using an integrating factor for the diffusive terms. The time-step  $dt$  is restricted by the CFL condition (with a coefficient of 0.1) and the penalisation stability condition (Kolomenskiy & Schneider 2009) which imposes  $dt < \eta$ . Laminar simulations were performed with  $128^3$  Fourier modes while turbulent simulations were performed with  $256^3$  modes. After dealiasing, provides  $85^3$  or  $171^3$  degrees of freedom remained. The penalisation parameter  $\eta$  was chosen to be  $5 \times 10^{-4}$ . It was verified that the results are consistent with those obtained using a resolution of  $256^3$  and/or using  $\eta = 1.25 \times 10^{-4}$ .

### 3. Circular Cross-section with Constant Axial Forcing

Let us first consider a cylinder with circular cross-section. The kinetic energy of the fluid is initially low, and, after a short time (a few Alfvénic time units, depending on the boundary forcing) the kinetic energy grows exponentially with no change in topology, which is consistent with the linear instability of helical modes as described in (Shan et al. 1991), before reaching a new steady state. In certain cases (low wrapping numbers / boundary forcing magnitude) this does not occur, and the kinetic energy is essentially zero for the duration of the simulation. Example kinetic-energy and kinetic energy dissipation curves are shown in Figure 3.

We set  $B_0 = 4.5$  and vary  $B_c$  so that integral values of wrapping numbers  $q$  are achieved. For  $q = 1$  no flow is observed. At  $q = 2$  ( $B_c \approx 7.06$ ) we observe a helical structure in the velocity field consisting of two pairs of helices, as shown in Figure 4. With these forcing parameters, the velocity modes have the same

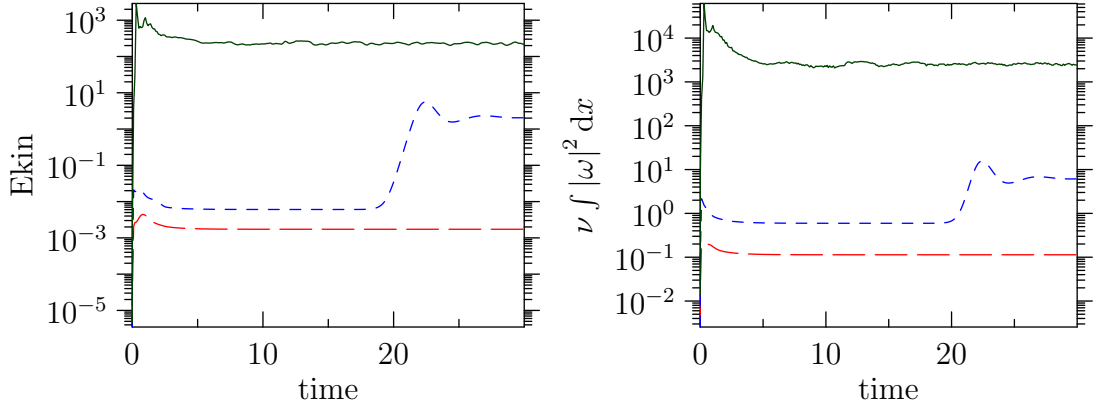


Figure 3: Kinetic energy as a function of time (left) and dissipation of kinetic energy as a function of time (right) for simulations in circular geometry with  $B_0 = 4.5$  and  $B_c \approx 3.53$  (red, long-dashed),  $B_c \approx 7.06$  (blue, short-dashed),  $B_c \approx 70.6$  (green, solid).

wrapping number as the boundary forcing of the magnetic field, which is also observed with wrapping number 3 ( $B_c \approx 10.6$ ). At wrapping number 4, the structure begins to break down, and is replaced with a helical dipole at  $q = 5$  ( $B_c \approx 17.6$ ), with wavenumber 2 in the axial direction, as shown in Figure 5. This low-order mode, which resembles the minimal dissipation mode as in (Montgomery, Phillips & Theobald 1989), endures even at  $q = 20$  (see Figure 6), at which point the velocity field in the  $z$ -direction is disordered and exhibits a full spectrum, as shown in Figure 7.

#### 4. Circular Cross-section with Varying Wrapping Number and Axial Field

In the previous section, we increased forcing by increasing the wrapping number to explore the effect on the topology of the flow. In order to understand the individual roles of forcing and wrapping number, we also perform a number of simulations with wrapping number  $q \in \{1, 2, 3, 4\}$  and various forcing amplitudes.

For wrapping number 1, we observe the formation of structures first at forcing amplitude  $B_{\parallel} = \sqrt{B_0^2 + B_c^2} = 20$ , consisting of two helical structures of opposite-signed axial velocity and axial wavenumber 1, matching the forcing wrapping number. This structure is also present for  $B_{\parallel} \in \{30, 40, 80, 100\}$ , and exhibits decreasing regularity as the forcing parameter increased. For wrapping number 2,

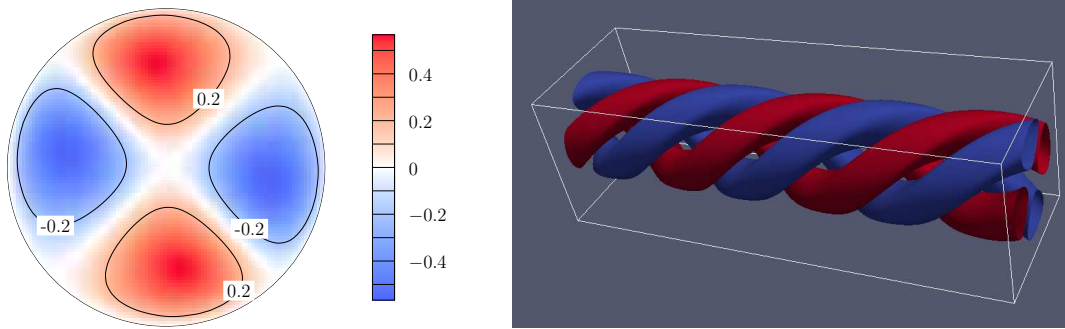


Figure 4: Axial velocity profile for wrapping number 2 with  $(B_0, B_c) = (4.5, 7.06)$  in a circular geometry. Left: the two-dimensional cut is taken at  $z = 4$ . Right: isosurfaces of  $u_z$  at  $\pm 0.2$ , which correspond to isocontours in the left image. The poloidal wavenumber of the helical structure is 2, and the axial wavenumber is 1, i.e., the  $(2, 1)$  mode dominates.

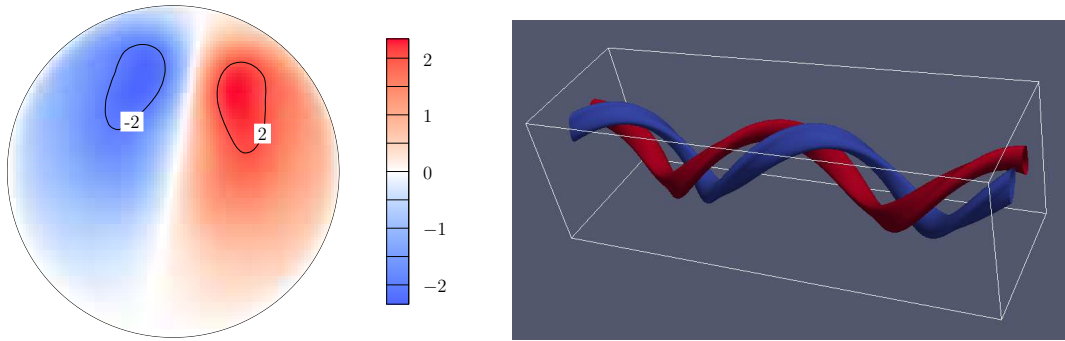


Figure 5: Axial velocity profile for wrapping number 5 with  $(B_0, B_c) = (4.5, 17.6)$  in a circular geometry. Left: two-dimensional cut taken at  $z = 4$ . Right: isosurfaces at  $u_z = \pm 2$ , showing a  $(1, 2)$  mode.

self-organisation occurs at lower forcing values, first appearing at  $B_{\parallel} = 10$ , at which point we observe three helical pairs, as shown in Figure 8. The structure of the flow becomes increasingly complex as  $B_{\parallel}$  increases, and an axial-wavenumber 1 mode appears at  $B_{\parallel} = 40$ , which persists up to  $B_{\parallel} = 100$ . At wrapping number 3, we observed axial-wavenumber 1 helical structures at  $B_{\parallel} \in \{30, 40, 60, 80, 100\}$ , with two helical pairs at low forcing degenerating into less ordered (but still helical) structures as forcing magnitude increased. Finally, simulations with  $q = 4$  show an axial wavenumber 2 helical pair at  $B_{\parallel} = 10$ , which, persists up to  $B_{\parallel} = 100$ . These results are summarised in Figure 9, which may be compared to Figure 1 in (Shan

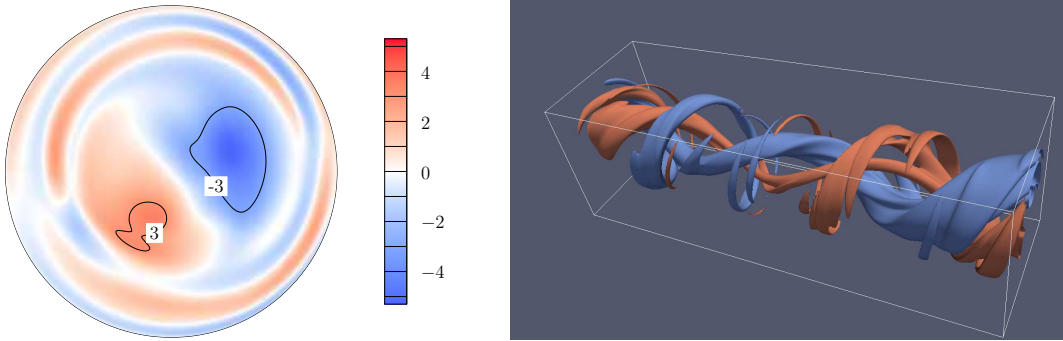


Figure 6: Axial velocity profile for wrapping number 20 with  $(B_0, B_c) = (4.5, 70.6)$  in a circular geometry at  $t = 20$ . Left: two-dimensional cut taken at  $z = 4$ . Right: isosurfaces at  $u_z = \pm 3$ , showing a central  $(1, 2)$  mode away from the boundary. An animation can be found in the supplementary material.

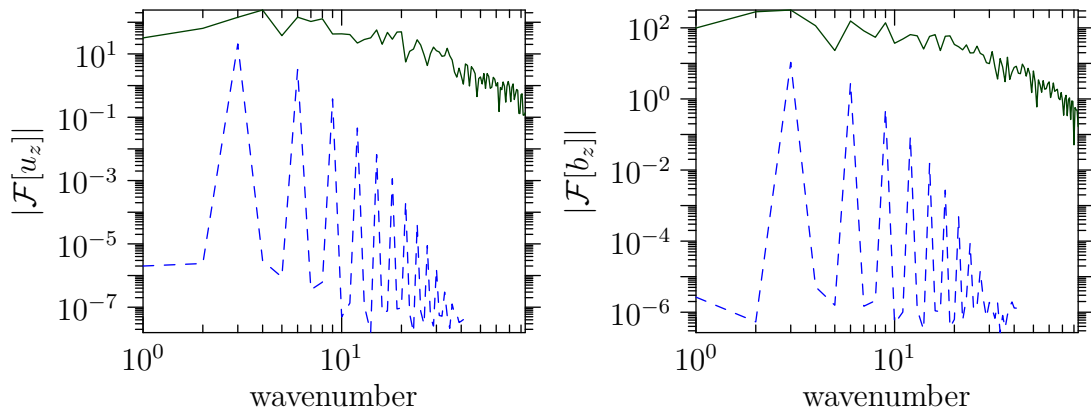


Figure 7: Power spectrum of the axial velocity (left) and axial magnetic field (right) at  $x = 0$ ,  $y \approx -0.37$  for the simulations shown in Figure 4 (blue, dashed line) and Figure 6 (green, solid line).

& Montgomery 1993b), which shows the linearly unstable modes as a function of pinch ratio  $\Theta = B_c/B_0$  and Hartmann number  $H = B_0/\sqrt{\eta\lambda}$  in a parameter region different than given here.

## 5. Alignment Statistics

In figure 10 we show the probability density functions (pdfs) of the cosine of the angles between  $(\mathbf{u}, \boldsymbol{\omega})$ ,  $(\mathbf{j}, \mathbf{B})$  and  $(\mathbf{u}, \mathbf{B})$ . These angles are chosen since they locally determine the strength of the Navier-Stokes nonlinearity, Lorentz force and

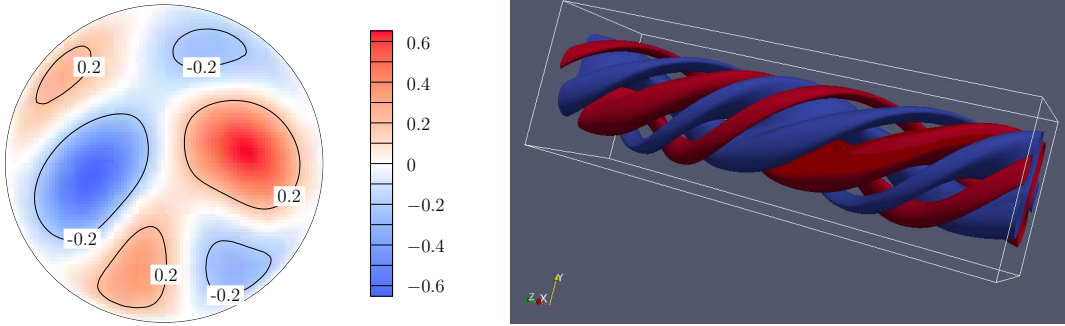


Figure 8: Axial velocity profile for wrapping number 2 with  $(B_0, B_c) = (8.28, 5.6)$  ( $B_{\parallel} = 10$ ) in a circular geometry. Left: two-dimensional cut taken at  $z = 6$ . Right: isosurfaces at  $u_z = \pm 0.2$ , showing a  $(3, 1)$  mode.

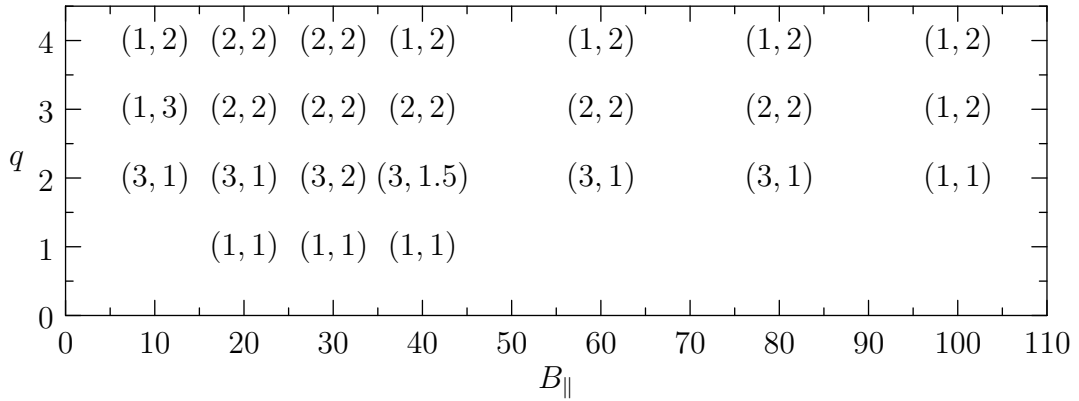


Figure 9: Mode diagram of the flow topology of helical modes observed at a given wrapping number  $q$  and forcing amplitude  $B_{\parallel}$ . Modes are  $(m, n)$ , where  $m$  is the poloidal mode number and  $n$  is the toroidal (axial) mode number.

magnetic field induction. Two cases are compared: a laminar one in which the velocity and magnetic field are stationary, and a turbulent multi-mode state. It is shown that already the laminar state shows non-trivial alignment properties. When the flow becomes turbulent the dynamics relax to a state in which in particular the magnetic field aligns more strongly with the velocity field compared to the laminar state. The  $\mathbf{u} - \boldsymbol{\omega}$  alignment becomes weaker and the  $\mathbf{j} - \mathbf{B}$  alignment does not dramatically increase or decrease in strength.

Such rapid local relaxation processes, in particular observed here for the  $\mathbf{u} - \mathbf{B}$  alignment have been observed previously in hydrodynamic (Pelz, Yakhot,

Orszag, Shtilman & Levich 1985) and magnetohydrodynamic (Servidio, Matthaeus & Dmitruk 2008) turbulence. In particular in the latter work similar alignments as the ones in the present work are investigated in the case of isotropic MHD turbulence. It is observed in their results that the  $\mathbf{j} - \mathbf{B}$  alignment becomes very strong. Furthermore, due to isotropy all their pdfs showed alignment-antialignment symmetry. This symmetry is lost in the pdfs of  $\mathbf{u} - \boldsymbol{\omega}$  and  $\mathbf{j} - \mathbf{B}$  of our simulations due to the imposed helical character of the magnetic field. We do not think that the alignment in the turbulent case can be explained in an easy way. However, it was suggested by (Kraichnan & Panda 1988) that the  $\mathbf{u} - \boldsymbol{\omega}$  alignment observed in isotropic turbulence might be one representation of a more generic property of turbulent systems to suppress their nonlinearity. The rapid relaxation observed in the present work can also be thought to be an expression of this property.

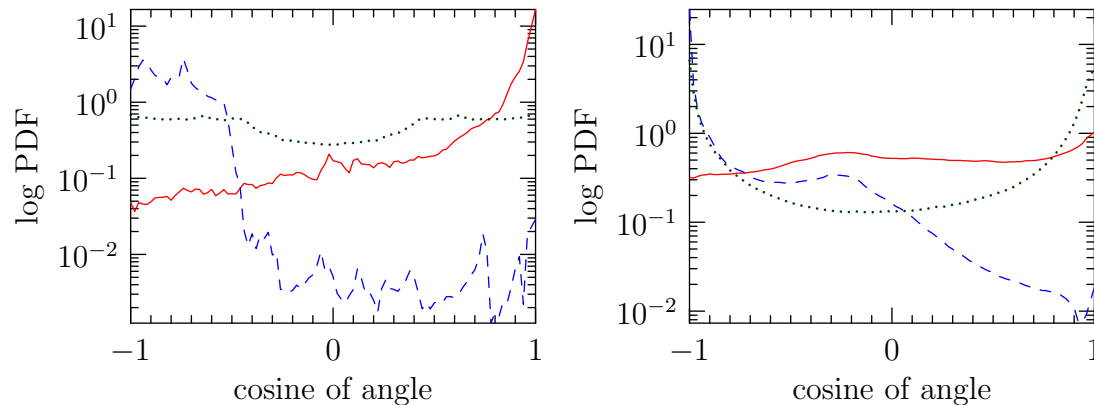


Figure 10: Probability distribution function for the cosine of the angle between  $\mathbf{u}$  and  $\boldsymbol{\omega}$  (red, solid),  $\mathbf{B}$  and  $\mathbf{j}$  (blue, dashed), and  $\mathbf{u}$  and  $\mathbf{B}$  (green, dotted) at  $t = 30$ . The left figure shows values for a laminar flow with  $(B_0, B_c) = (4.5, 7.06)$ , and the right figure is for a turbulent flow with  $(B_0, B_c) = (4.5, 70.6)$ .

## 6. Elliptical Cross Section

Let us now consider a cylinder with elliptical cross section defined by  $x^2 + 2y^2 = 1$ . As in the previous section, we keep the wrapping number constant and modify the forcing magnitude. The onset of kinetic energy growth occurs at much stronger forcing than in the circular case, with  $q = 1$ ,  $B_{\parallel} = 60$  our first detection. At this point, the velocity field forms five pairs of opposite-sign helices, as shown in

Figure 11. As forcing is increased, 6 pairs are observed at  $B_{\parallel} = 80$ , and 5 pairs again at  $B_{\parallel} = 100, 110, 120$ , and  $130$ . As forcing amplitude is increased, the velocity field becomes increasingly concentrated at the border.

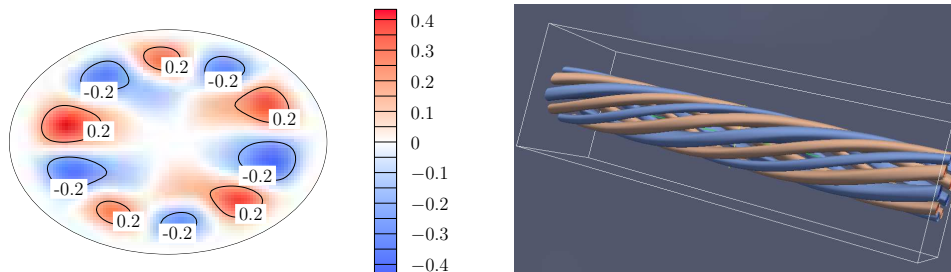


Figure 11: Axial velocity profile for wrapping number 1 with  $(B_0, B_c) = (49.7, 33.6)$  ( $B_{\parallel} = 60$ ) in an elliptical geometry. Left: two-dimensional cut at  $z = 4$ . Right: isosurfaces at  $u_z = \pm 0.2$ , showing a  $(5, 1)$  mode.

## 7. Conclusion

In this article we studied the self-organisation of the flow in a conducting fluid confined in a cylinder. The flow is forced by a helical magnetic field imposed via boundary conditions. This phenomenon was first explored by Shan et al. using a purely spectral method for circular cross-sections with non-penetration boundary conditions. The simulations presented here used a large number of grid points, different parameter regimes, and were performed in cylinders with both circular and elliptical cross-sections. The penalisation technique can also be used in more general geometries. In cylinders of circular cross-section, various helical flows develop depending on the value of the wrapping number and forcing amplitude, tending toward a unique low-order mode at large values of the forcing parameters. This mode is present even when the fluid starts to exhibit turbulent dynamics. For the elliptical cross-section, the situation is different: a ring of vortices with poloidal mode number 5 or 6 forms and encloses a weak flow area. These vortices follow the topology of the imposed magnetic field. The magnitude of the forcing required to trigger this instability is much larger than for circular case. For further work, it would be interesting to study the flow for larger ranges of Hartman number and pinch ratio, and to investigate the influence of the eccentricity of the ellipse on the topology of the flows obtained. Indeed, these first results in cylinders with non-circular cross-section show significant influence of the shape on

the modes which are excited. This observation might have important implications for the control of Reversed Field Pinch fusion reactors, where the shape and frequency of the helically extended modes determines the quality of the plasma confinement. Even though in realistic RFP simulations the strong temperature gradient will have an important influence on the dynamics, already the isothermal visco-resistive MHD description is shown to reproduce a number of key features of the dynamics (Bonfiglio et al. 2013).

## Acknowledgments

This work was supported by the contract SiCoMHD (ANR-Blanc 2011-045), with simulations performed on IDRIS under project 91664 and made use of the HPC resources of Aix-Marseille Université financed by the project Equip@Meso (ANR-10-EQPX-29-01) of the program ‘‘Investissements d’Avenir’’ supervised by the ANR.

## Appendix A. Numerical method for producing a solenoidal penalisation field

Let  $\Omega = \Omega_f \cup \Omega_s$  be the computational, fluid, and solid domains, respectively, with  $|\Omega_f \cap \Omega_s| = 0$ . Given a Dirichlet boundary condition on  $\partial\Omega_f$  represented by  $\{\mathbf{v}_{bc}(\mathbf{x}) | \mathbf{x} \in \partial\Omega_f\}$  such that

$$\int_{\partial\Omega_f} \mathbf{v}_{bc} \cdot \mathbf{n} \, ds = 0, \quad (\text{A.1})$$

where  $\mathbf{n}$  is the normal vector on  $\partial\Omega_f$ . We wish to extend  $\mathbf{v}_{bc}$  to a sufficiently regular function  $\mathbf{v}$  on the entire computational domain  $\Omega$  such that  $\nabla \cdot \mathbf{v} = 0$ . In order to find  $\mathbf{v}$  numerically, we introduce a pseudo-time  $\tau$  and time-step the equation

$$\frac{\partial \mathbf{v}}{\partial \tau} = \kappa \nabla^2 \mathbf{v} - \frac{1}{\eta_\tau} \chi_{\partial\Omega_f} (\mathbf{v} - \mathbf{v}_{bc}) \quad (\text{A.2})$$

where  $\kappa$  is a diffusion parameter,  $\chi_{\partial\Omega_f}$  is the characteristic function for  $\partial\Omega_f$ , and we call  $\eta_\tau$  the pseudo-time penalisation parameter. For the simulations in this paper, we chose  $\kappa = 100$ , and we used an adaptive 1<sup>st</sup>/2<sup>nd</sup> order embedded Runge–Kutta time-integrator and a pseudospectral method in space, projecting  $\mathbf{v}$  onto the solenoidal manifold via a Helmholtz decomposition after each time-step. The time-stepping in  $\tau$  is stopped when

$$\|\mathbf{v}_{bc} - \mathbf{v}\|_{\infty, \partial\Omega_f} < 0.2 \times \sqrt{\eta}, \quad (\text{A.3})$$

where  $\eta$  is the penalisation parameter used to advance the fluid. This is to say that the maximum error between the penalisation field  $\mathbf{v}$  and the desired value  $\mathbf{v}_{bc}$  on the boundary is less than one fifth the error expected from the penalisation term used in time-stepping the fluid. Since the boundary conditions obey the compatibility condition (equation (A.1)), the resulting field is consistent with a solenoidal field and should not be affected by projection onto the solenoidal manifold. Moreover, the stopping condition (inequality (A.3)) is satisfied only when the resulting penalisation field closely matches the boundary conditions.

The stop condition A.3 implies that the error in the boundary conditions is sub-leading-order, and the use of a Helmholtz decomposition provides a penalisation field which is divergence-free up to machine precision. The choice of  $\kappa$  determines the regularity of the field and the number of time-steps required for condition A.3 to be achieved.

## References

- Angot, P., Bruneau, C.-H. & Fabrie, P. (1999), ‘A penalization method to take into account obstacles in incompressible viscous flows’, *Numerische Mathematik* **81**(4), 497–520.
- Arquis, E. & Caltagirone, J.-P. (1984), ‘Sur les conditions hydrodynamiques au voisinage d’une interface milieu fluide—milieux poreux: application à la convection naturelle’, *Comptes-Rendus de l’Académie des Sciences* **299**, 1–4.
- Bonfiglio, D., Veranda, M., Cappello, S., Escande, D. & Chacón, L. (2013), ‘Experimental-like helical self-organization in reversed-field pinch modeling’, *Physical Review Letters* **111**(8), 085002.
- Bos, W. J. T., Neffaa, S. & Schneider, K. (2008), ‘Rapid generation of angular momentum in bounded magnetized plasma’, *Physical Review Letters* **101**(23), 235003.
- Canuto, C., Hussaini, M. Y., Quarteroni, A. & Zang, T. A. (1988), *Spectral methods in fluid dynamics*, Springer-Verlag.
- Horiuchi, R. & Sato, T. (1986), ‘Self-organization process in three-dimensional compressible magnetohydrodynamics’, *Physics of Fluids (1958-1988)* **29**(12), 4174–4181.
- Kolomenskiy, D. & Schneider, K. (2009), ‘A Fourier spectral method for the Navier–Stokes equations with volume penalization for moving solid obstacles’, *Journal of Computational Physics* **228**(16), 5687–5709.
- Kraichnan, R. H. & Panda, R. (1988), ‘Depression of nonlinearity in decaying isotropic turbulence’, *Physics of Fluids (1958-1988)* **31**(9), 2395–2397.
- Moffatt, H. K. (1978), *Magnetic Field Generation in Electrically Conducting Fluids*, Cambridge University Press.
- Montgomery, D., Phillips, L. & Theobald, M. (1989), ‘Helical, dissipative, magnetohydrodynamic states with flow’, *Physical Review A* **40**(3), 1515.
- Morales, J., Bos, W., Schneider, K. & Montgomery, D. (2012), ‘Intrinsic rotation of toroidally confined magnetohydrodynamics’, *Physical Review Letters* **109**(17), 175002.
- Morales, J., Leroy, M., Bos, W. & Schneider, K. (2012, revised), ‘Simulation of confined

- magnetohydrodynamic flows using a pseudo-spectral method with volume penalization', *Journal of Computational Physics, revised* .  
**URL:** <http://hal.archives-ouvertes.fr/hal-00719737>
- Neffaa, S., Bos, W. J. T. & Schneider, K. (2008), 'The decay of magnetohydrodynamic turbulence in a confined domain', *Physics of Plasmas* **15**, 092304.
- Pelz, R. B., Yakhot, V., Orszag, S. A., Shtilman, L. & Levich, E. (1985), 'Velocity-vorticity patterns in turbulent flow', *Physical review letters* **54**(23), 2505.
- Servidio, S., Matthaeus, W. & Dmitruk, P. (2008), 'Depression of nonlinearity in decaying isotropic mhd turbulence', *Physical review letters* **100**(9), 95005.
- Shan, X. & Montgomery, D. (1993a), 'On the role of the hartmann number in magnetohydrodynamic activity', *Plasma physics and controlled fusion* **35**(5), 619.
- Shan, X. & Montgomery, D. C. (1993b), 'Global searches of Hartmann-number-dependent stability boundaries', *Plasma Physics and Controlled Fusion* **35**, 1019.
- Shan, X., Montgomery, D. C. & Chen, H. (1991), 'Nonlinear magnetohydrodynamics by Galerkin-method computation', *Physical Review A* **44**(10), 6800–6818.
- Taylor, J. B. (1974), 'Relaxation of toroidal plasma and generation of reverse magnetic fields', *Physical Review Letters* **33**(19), 1139.
- Veranda, M., Bonfiglio, D., Cappello, S., Chacón, L. & Escande, D. (2013), 'Impact of helical boundary conditions on nonlinear 3d magnetohydrodynamic simulations of reversed-field pinch', *Plasma Physics and Controlled Fusion* **55**(7), 074015.
- Wesson, J. (2011), *Tokamaks*, Vol. 149, Oxford University Press.
- Zhu, S.-p., Horiuchi, R., Sato, T. et al. (1995), 'Non-taylor magnetohydrodynamic self-organization', *Physical Review E* **51**(6), 6047.